Journal of Ceramic Processing Research. Vol. 23, No. 4, pp. 523~528 (2022)
(Received 21 January 2022, Received in revised form 27 May 2022, Accepted 4 June 2022)
https://doi.org/10.36410/jcpr.2022.23.4.523

J O U R N A L O F
Ceramic Processing Research

Parameter optimization in Laser Beam Welding for Incoloy 825 Ni-based alloy and AISI 316L steel

S. Srikanth[a], A. Parthiban[b,*], M. Ravikumar[c] and K. Vignesh[d]
[a]*Research Scholar, Department of Mechanical Engineering, Vels Institute of Science, Technology & Advanced Studies Pallavaram,Chennai – 600117*
[b]*Associate Professor, Department of Mechanical Engineering, Vels Institute of Science, Technology & Advanced Studies. Pallavaram, Chennai - 600117*
[c]*Professor, Department of Mechanical Engineering, Bannari Amman Institute of Technology, Sathyamangalam – 638401*
[d]*Assistant Professor, Department of Mechanical Engineering, PSNA College of Engineering and Technology, Dindigul – 624622*

This paper investigates the comparative study on dissimilar joints of Incoloy 825 Ni-based alloy and AISI 316L steel. The paper explores process parameters such as laser focal diameter, strength, and pulse frequency of the above dissimilar plates in LBW welding. In order to explain the microstructural changes during welding, characterization was carried out by optical microscopy and electron microscopy. In order to study the transformation of mechanical properties in solder joints, micro-hardness and tensile tests are performed. Based on the research work, due to its less heat affected area, high power strength, and high repetition rate, laser beam welding has some advantages over other welding techniques. The Taguchi method is more efficient for predicting the outcomes among different analytical and experimental optimization methods. Therefore, this experiment demonstrates that different metals' welding efficiency can fulfil the oil and gas sector standards and other industrial sectors.

Keywords: Optimization, Ni-Alloy, Incoloy825, Dissimilar welding, Nd:YAG.

Introduction

In the oil and gas industry, where sulphuric and nitric acid use is strong, this nickel alloy 825 and 316L SS are used. These products are used in heat exchangers, boilers, the food industry, and in fields such as workplaces for emission control boards, oil and gas recovery, chemical refining stations, acid production plants, etc. They are ideally suited to the aquatic environment because they are extremely resistant to marine water corrosion. Also, to maintain adequate rigidity, ductility, and corrosive resistance at low temperatures, LNG pipelines are required [1]. This mixture of nickel alloy 825 and 316L SS is also ideally matched to the specifications. The crevice corrosion and pitting corrosion tests demonstrate that UNS N08825 (alloy 825) has high localized corrosion resistance caused by chloride [2].

This work models magnetically aided welding using SmCo26 permanent magnets in 316L stainless steel, thus offering a complete description of the heat transfer phenomenon and subsequent demagnetization. For minimum demagnetization and optimum magnetic field in the melt pool, the number of magnets, the direction of their poles, and their location relative to the weld are optimized. Its critical pitting temperature and crevice corrosion temperature in polluted chloride seawater are considerably higher than in alloy N08028 (alloy 28) and UNS N06625 (alloy 625) due to its high chromium and molybdenum concentration [3]. Various parametric parameters such as welding speed, laser strength, focal position, and pulse frequency investigated Nd's effect: YAG pulsed laser-welded super-duplex stainless steel (SDSS). Two separate models measure tensile stress, and the ductile fracture and smaller grains characterise the tensile fracture [4]. The investigated Co2 laser welding, in which heating effects are enhanced with a pulse time increase for a given average power, travel speed, and APPD, increased with higher APPD, enabling materials to be operated by laser welding [5]. For copper and aluminium, the laser diode-pumped Nd:YAG (maximum output of 4.4 kW) is commonly used. It is used to detect the effect of process parameters depending on the ability of the laser welders and decide the copper and aluminium soldering is optimised by silicone in aluminium [6]. This paper explains how solidification creates a 100 percent austenite microstructure, as seen by EBSD scans using a standard Gaussian beam. In the arrangement, however, chromium, molybdenum, and sulfur microsegregation are visible at the cells' outer edges. Where a diffractive optical

*Corresponding author:
Tel : +9578961066
E-mail: parmathi83@gmail.com

element utilizes a uniform distribution of irradiance, a partially austenitic structure is formed by the fusion region [7]. The size of the grain remains (200 μm), but the ferrite is reduced as well. It may be due to higher quench strength using the distribution of square uniform irradiance [8]. These studies indicate that process parameters greatly impact the cooling speed because of the different soldering power and soldering length [9]. As the solder power was elevated and the solder velocity was decreased, the heat-affected zone and fusion zone were observed. In this analysis, an important finding can be obtained that the average temperature rise is smaller than the upper limit of heat consumption [10]. In this analysis, proper welding conditions were observed for the bellows attachment and the flanged joint of an expansion joint with STS316L and INCOLOY 825 materials. Of INCOLOY 825, the hardness of the base metal was 200 to 210 Hv, but the hardness of the solder improved to 220 to 330 Hv because, after soldering, the structure became more microscopic. Thanks to the two-pass soldering, however, the single-pass welding value was low; the soldering was slow [11]. The geometric features of the bead play an important role in deciding the accuracy of each weld joint, taking into consideration its meaning, i.e., bead middle, bead volume, and the key effects of performance responses on variables of change control. A critical function is played by the bead functionality [12]. High homogeneous solidification forms at AISI 304-AISI 1020 dissimilar welding through electric resistance spot welding. The weld current also influenced the tensile strength and nugget diameter [13]. The influence of input welding process parameters on the performance characteristics of the welded specimen was explored using experimental dissimilar metal friction stir welding. The affecting characteristics were found to be tool rotating speed, which considerably improved the specimen's microhardness by 12.86% over the base aluminium 5083-H32 alloy [14].

For the experimental data gathered, RSM is used, and models for adequacy checking for each output response are predicted. By measuring the patterns between input and reference parameters, the diagrams are also analyzed. It is also possible to use the RSM models to optimize the operation. The options for welding small parts are known as TIG and MIG welding. But it does take ability and has some pitfalls. Ni-based alloys for welding are shown to help high-energy laser beam welding. Welding is carried out to produce a high-quality weld by a sequence of short bursts that heat the metal. Efforts are then undertaken to use laser beam welding Nd: YAG to connect nickel alloys 825 and 316L SS and examine microstructural changes in the welded region.

Materials Selection

Grade 316 Stainless steel

With the significance of 304, Grade 316 is the second of the austenitic stainless steel to carry the regular molybdenum. Complete molybdenum corrosion resistance properties are 316 higher than grade 304; this is especially highly resistant to pitting and cracking in chloride environments. Rate 316L, low carbon 316, and resistance to sensitivity variant (precipitated carbide grain boundary). It is also widely used in heavy welded gauge parts (around 6 mm). Often, there is no major price difference between 316 and 316L stainless steel. Also, at cryogenic temperatures for these groups, the austenitic structure is still very robust. At high temperatures, 316L stainless steel gives higher creep, rupture stress, and tensile strength than austenitic stainless steel chromium-nickel. The chemical and mechanical properties of 316L stainless steel are illustrated in Tables 1 and 2.

Grade 316L is more resistant to carbide and can be used at high temperatures. At high temperatures, Grade 316H has greater power, some of which is added to structural and pressure-containing applications at a temperature of over 500 C. The standard “sea grade stainless steel” is commonly considered 316 but is not resistant to warm marine water. 316 shows surface degradation in certain aquatic habitats, typically evident in brown coloring. The resulting tears and rough surface finish are mostly related by normal fusion and resistance techniques to excellent weldability with and without filler metals. Major soldered sections in Grade 316 require post-solder annealing for maximum corrosive resistance. This method was not appropriate for the use of stainless steel 316L oxyacetylene soldering techniques.

Incoloy825 Ni-Based Alloy

The extraordinary property of Incoloy 825, seen in Table 3, is corrosion resistance. As degraded and oxidized, rust, pitting and cravings, intergranular degradation, and stress cracking are stopped by Incoloy 825. It is particularly useful in the treatment of sulphuric and

Table 2. SS 316L Mechanical properties

S.No	Properties	Range
1	Tensile stress (MPa)	485-545
2	Yield stress(MPa)	140-200
3	Elongation (%)	36-50
4	Hardness (HB)	212-250

Table 1. Stainless steel-316L Chemical Properties

Composition	N	Ni	C	Mn	Si	P	S	Cr	Mo
Percentage (%)	0.1	10.5- 14.5	0.025-0.03	1-2	0.70-0.75	0.040	0.01-0.03	15-20	2-4

Table 3. Chemical properties of Incoloy 825

Grade	Ranges (%)
Fe	20-22
Ni	30- 45
C	0.025-0.03
Mn	1-2
Si	0.30-0.5
Mb	2-4
S	0.01-0.03
Cr	19-25
Al	0.1-0.3

phosphoric acids, flue gases, saline gases, oil wells, and sulfur-containing marine waters.

In industrial devices, vehicles, valves, cars, semiconductive machinery, flow and pressure sensors, and even aircraft are commonly used. Because conventional fossil fuels have recently been exhausted, natural liquefied petroleum is needed more than ever as alternative oil, increasing the need for bellows on LNG vessels. As a material for LNG bellows, the alloys SS316L and INCOLOY 825 are resistant to corrosion and low-temperature fragility. SS316L is low-carbon stainless steel with a carbon content of less than 0.03 percent that prevents intergranular corrosion by welding and maintains low-temperature strength and control. The purpose of this analysis is to develop the best welding specifications for INCOLOY 825 and SS316L special materials for use at low temperatures and test the durability of the product. To this end, we demonstrate that the optimal welding conditions are ideally fit for joining the steel.

Methodology

Laser beam welding

The soldering process is done by ECO 2600 Pulsed laser beam welding. In particular, this recent invention provides an inexpensive introduction to laser welding for small businesses and young companies taking the initial steps in this field. Of note, the laser soldering system is also suitable for professionals who want to improve their soldering skills. It is lightweight and

Fig. 1. Laser beam welding.

compact and can be ready for use easily and deeply durable, including tools and die production, to meet increasing customer requirements. No sacrifice was made in the sense of customer experience, in particular. The 150 kg motor-controlled table (x / y / z) makes synchronous laser axis welding, which is also valid for four axes for the motorized rotor axis seen in Fig. 1.

Taguchi analysis

A new approach for conducting studies based on simple principles has been suggested by Taguchi. A special array called orthogonal array is used in this method. A limited number of experiments are listed in these regular arrays so that all variables influencing the output parameter can be completely defined, as seen in table 4. In order to explain the effects of three different variables, each with three-factor levels, the orthogonal array L9 is planned. This list implies that two variables cannot communicate. While there is no presumption in many situations that the interaction model is true, there are cases where there is strong proof of interaction. A common interaction will be the interaction between material properties and temperature, the microstructural view used to examine the affected welding region from welded plating is seen in Fig. 2.

Fig. 2. Dissimilar material welded by laser beam welding

Table 4. Parameters selection for Taguchi analysis

Specimen No.	Laser Dia. Mm	Power W	Frequency Hz
1	0.3	45	8
2	0.3	44	9
3	0.3	46	10
4	0.4	44	9
5	0.4	45	10
6	0.4	46	8
7	0.5	44	10
8	0.5	45	8
9	0.5	46	9

A research procedure for testing means variations between two or more therapies is the hypothesis. Even where more than one unit is used to duplicate duplication, mathematical reasoning also makes it easier. The researcher increases the chances of helping to discover improvements in the experimental phase. You will find the optimal welding conditions for the best welding here.

Results and Discussion

Mechanical behaviors

The average durability of the base metal is 230 HV, as shown in Table 5. Compared to the interface and the base material, hardness values are higher in the fusion soldering area. The sold machine's strength in the middle, cap, and root were 195, 198, and 197 HV. Compared to all the other areas, the primary material area is softer, and therefore tensile failure can occur in the weaker portion of the base material. The ANOVA table's findings for selecting the best three specimens show that the 9th individual specimen has a higher-yielding intensity, an elongation of about 15.5%, and the addition of a tensile test caused a fracture in the parent métal. This canbe achieved with 9 specimens out of 3 specimens with the highest hardness tests and microstructure.

Metallurgical analysis

No detectable defects on the welding surface of the sold bead or adjacent areas at the intersection of the welding joint are noticeable in the relevant field. Due to the specimen welded in energy 2.5 J and even welded beads, the welding properties of the pulsed laser beams suggest no welding crises between the two components, and this may occur due to stainless steel 316L, and Incoloy 825 has a normal tolerance to crashes as well as optimal soldering parameters. The metal sold does not indicate any discontinuity. The gas shielding's effectiveness is demonstrated to withstand oxidation, high porosity, and incorporation of gas and gas. Direct heating and energy delivery are both laser-welded in the conduction mode. The SS316L and Incoloy microstructure studies are shown in Figs. 3 and 4. The absorption of the beam energy by the material surface was included in the direct heating process. In Fig. 5, the laser strength stimulates some of the minute surface shoes, the 9th weld region's microstructure, and the heat-affected area.

Fig. 3 shows the Microstructural view of Incoloy 825, normally Ni alloy has high nickel and chromium content for high strength. The image shows there is no defect over the Ni alloy material surface. Fig. 4 shows the microstructural view of stainless steel 316L, which

Table 5. Mechanical behaviors of welded specimen

Specimen No.	Hardness HV	Tensile Strength MPa
1	164	216
2	199	364
3	204	381
4	177	211
5	185	235
6	346	416
7	213	237
8	162	211
9	425	423

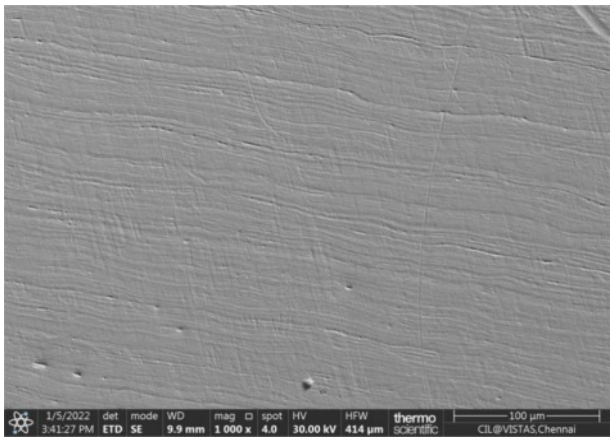

Fig. 3. Microstructure analysis of Ni-alloy.

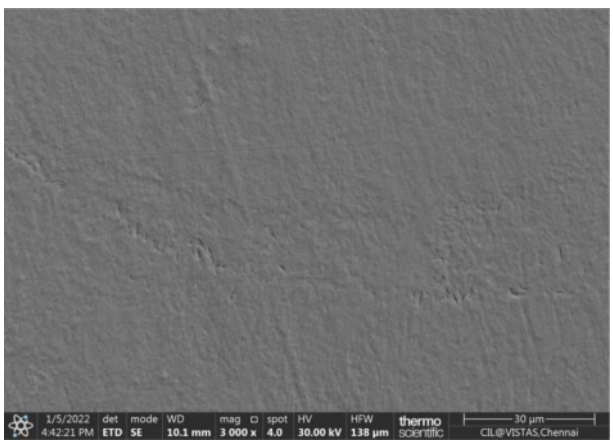

Fig. 4. Microstructure analysis of Stainless Steel.

has high Chromium content (17%) to increase the strength and reduce corrosion.

Fig. 5 shows the welding zone between the Incoloy 825 and stainless steel 316L, here the hard surface indicates the Incoloyand the smooth surface indicate the stainless steel 316L.

Compare with other welding processes laser welding has an effective and fast process. The Heat Affected Zone is slightly formed in Incoloy 825 Ni-based alloy and AISI 316L steel welding shown in Fig. 6.

They were both laser-welded in the direct mode of heating and energy transfer. Beam strength absorption by the surface of the material was used in the direct heating mechanism. The high power of the laser is the source of many small surface holes. Fig. 6 shows the 9th welding zone's microstructure, the heat zone, and the fusion zone.

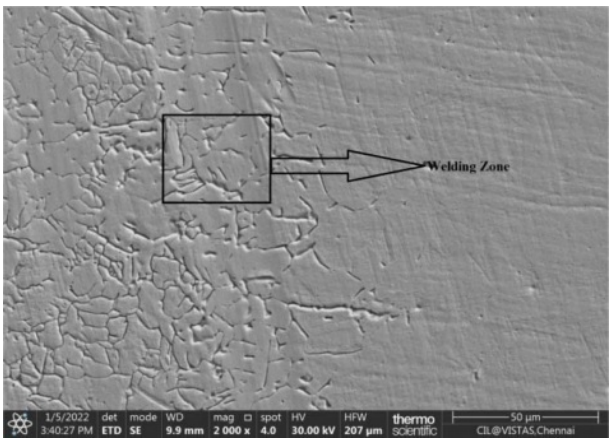

Fig. 5. Microstructure analysis of Welding zone.

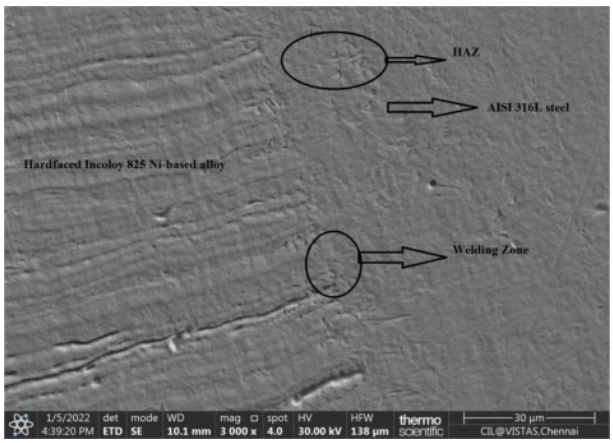

Fig. 6. Microstructural Analysis of Incoloy 825 Ni-based alloy and AISI 316L steel.

ANOVA Table

The L9 orthogonal array was made from the test value using the 7.0 architecture expert program, and the ANOVA Table 6 was shown below.

Form 7.48's F-value suggests that the model is essential. A value below 0.0500 “Prob> F” indicates important model words.

Fig. 7 above indicates that strength has played an important part in tensile strength. If the tensile strength of the laser beam increases, tensile strength increases progressively. In the same case, the production increases from 44W to 46W. From 188 MPa to 510 MPa, the tensile capacity rose significantly. The rate of growth in tensile strength varies slightly. The resistance to traction is not compromised.

It is apparent from Fig. 8 above that there is a small shift in tensile power. The Incoloy 825 and AISI 316L weld plate's tensile strength was not compromised by laser diameter and wavelength. In tensile power, only minor variations arise.

It is apparent from Fig. 9 above that power plays an essential role in tensile strength. There is a progressive

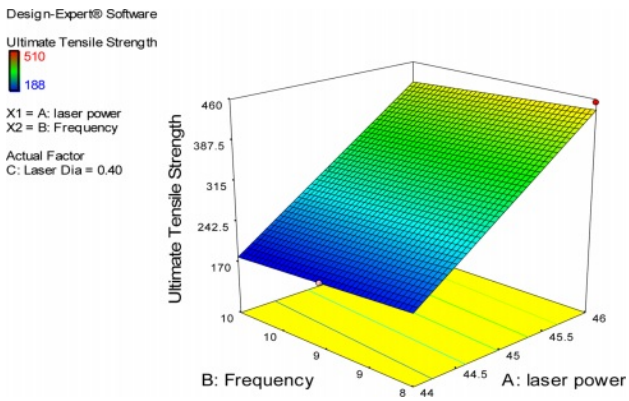

Fig. 7. Laser power vs. Frequency on Tensile Strength.

Table 6. Analysis Of Variance Table

ANOVA for Response Surface Linear Model					
Analysis of variance table [Partial sum of squares - Type III]					
Source	Sum of Squares	Df	Mean Square	F Value	p-value Prob> F	
Model	89237.5	3	29743.5	7.484184	0.0268	Significant
A-laser power	88463.5	1	88572.5	22.28759	0.0051	
B-Frequency	603	1	603	0.150968	0.7135	
C-Laser Dia	53	1	53	0.013578	0.9116	
Residual	19840.5	5	3973.1			
Cor Total	109089	8				

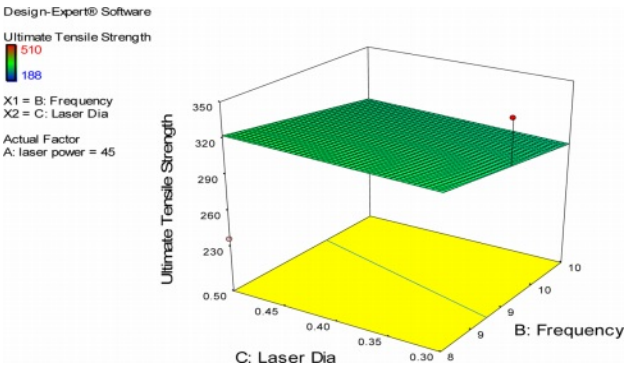

Fig. 8. Laser Dia. Vs. Frequency of Tensile Strength.

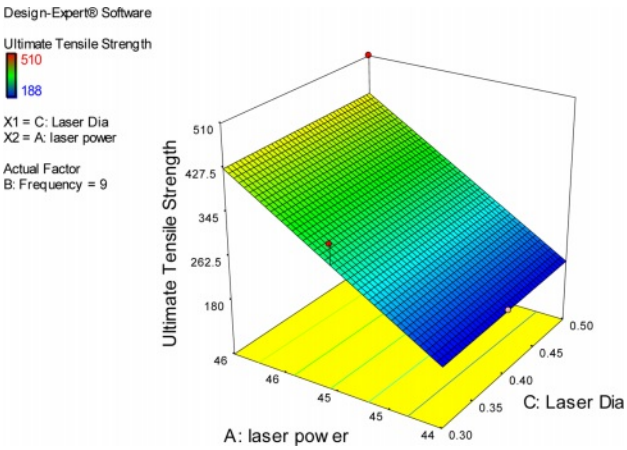

Fig. 9. Laser power Vs. Laser Diameter on Tensile Strength.

increase in tensile strength as the laser diameter of the laser beam increases. In the same case, there is a dramatic improvement in tensile strength from 188 MPa to 510 MPa from 44 W to 46 W. From the above results, it is concluded that strength plays a major role in increasing the welded samples' tensile values. The remaining two parameters have a relatively low effect.

Tensile strength = -5078.16 + 31 *laser diameter + 120.4*Power + *-11 Frequency is the mathematical model observed from ANOVA table.

Conclusion

The INCOLOY 825 and SS316L materials have high corrosion resistance and outstanding mechanical properties. In the oil and gas industry, marine systems, find acceptable applications. For its accuracy and precision, laser beam welding was selected, and it also has the least heat-affected zone relative to other welding methods. In order to find the best parameters for our welding operation, we chose the L9 Orthogonal form. We only select 3 parameters for the analytical purpose of this analysis. We made 9 specimens for our investigations using these 3 parameters; it is inferred from the experimental analysis that major changes were observed.

The optimized parameters are 0.5mm beam diameter, 46 W power, and 9Hz frequency from Taguchi's L9 Orthogonal Optimization Procedure, which gives the maximum Tensile Strength to the welded samples of SS316L and INCOLOY 825 using the Nd:YAG Pulsed Laser Beam Welding Process and its advantages and limitations are shown below. Laser intensity played an important role in material welding as a result of the ANOVA study.

Higher hardness values have been established that are sufficient for the weld's functional dimensions in the practical area of operation.

Laser welding provides a high-quality weld and provides a good penetration depth for greater power. From the 9th specimen, a high tensile value of 510Mpa was obtained.Failure occurs at the welded joint because of the pores generated due to the 1mm depth of penetration.

References

1. J. Kangazian, and M. Shamanian, J. Manuf. Process.26 (2017) 407-418.
2. J. Kangazian, M. Shamanian, and A. Ashrafi, J. Manuf. Process. 29 (2017) 376-388.
3. D. Aravindkumar, and R. Thirumalai, Mater. Res. Express 8[4] (2021) 046513.
4. S. Sharma, M. Chandrasekaran, and R. Thirumalai, Manuf. Technol. Today 13[6] (2014) 20-29.
5. J.P. Oliveira, N. Schell, N. Zhou, L. Wood, and O. Benafan, Mater. Des. 162 (2019) 229-234.
6. N. Sayyar, M. Shamanian, and B. Niroumand, J. Mater. Process. Technol. 262 (2018) 562-570.
7. N.R. Bijivemula, and G. Padmanabhan, Adv. Mater. Process. Technol. (2021) 1-16.
8. N. Kumar, M. Mukherjee, and A. Bandyopadhyay, Opt. Laser Technol. 94 (2017) 296-309.
9. N. Ghosh, P.K. Pal, and G. Nandi, ProcediaTechnol. 25 (2016) 1038-1048.
10. M.R. Pakmanesh, and M. Shamanian, Opt. Laser Technol. 99 (2018) 30-38.
11. P.G. Krishnan, B.S. Babu, and K. Siva, J. Ceram. Process. Res. 21[2] (2020) 157-163.
12. P.G. Krishnan, B.S. Babu, S. Madhu, S.J. Gowrishankar, C. Bibin, S. Saran, S.S. Ram, A.R. Hari and S. Vidyasagar, J. Ceram. Process. Res. 22[5] (2021) 483-9.
13. M. Kannaiyan, J.G. Raghuvaran, K. Govindan and E.P. Annamalai, J. Ceram. Process. Res. 21[1] (2020) 26-34.
14. R. Crushan and P. AshokaVarthanan, J. Ceram. Process. Res. 22[6] (2021) 620-628.